3-14-2012

Size and Support Effects for the Water-Gas Shift Catalysis over Gold Nanoparticles Supported on Model Al2O3 and TiO2

Mayank Shekhar
Purdue University, mayankshekhar@purdue.edu

Jun Wang
Purdue University

Wen-Sheng Lee
Birck Nanotechnology Center, Purdue University, wenshenglee@purdue.edu

W. Damion Williams
Purdue University, wdwillia@purdue.edu

Seung Min Kim
Birck Nanotechnology Center, Purdue University

See next page for additional authors

Follow this and additional works at: http://docs.lib.purdue.edu/nanopub

Part of the Nanoscience and Nanotechnology Commons

Authors

Mayank Shekhar, Jun Wang, Wen-Sheng Lee, W. Damion Williams, Seung Min Kim, Eric A. Stach, Jeffrey T. Miller, W. Nicholas Delgass, and Fabio H. Ribeiro

Size and Support Effects for the Water−Gas Shift Catalysis over Gold Nanoparticles Supported on Model Al_2O_3 and TiO_2

Mayank Shekhar,[†] Jun Wang,[†] Wen-Sheng Lee,[†] W. Damion Williams,[†] Seung Min Kim,[‡,§,#] Eric A. Stach,[‡,§,⊥] Jeffrey T. Miller,[∥] W. Nicholas Delgass,[†] and Fabio H. Ribeiro*,[†]

[†]School of Chemical Engineering, and [‡]School of Materials Engineering, Purdue University, West Lafayette, Indiana 47907, United States

[§]Birck Nanotechnology Center, West Lafayette, Indiana 47907, United States

[∥]Chemical Sciences and Engineering Division, Argonne National Laboratory, Argonne, Illinois 60439, United States

Ⓢ *Supporting Information*

ABSTRACT: The water−gas shift (WGS) reaction rate per total mole of Au under 7% CO, 8.5% CO_2, 22% H_2O, and 37% H_2 at 1 atm for Au/Al_2O_3 catalysts at 180 °C and Au/TiO_2 catalysts at 120 °C varies with the number average Au particle size (d) as $d^{-2.2\pm0.2}$ and $d^{-2.7\pm0.1}$, respectively. The use of nonporous and crystalline, model Al_2O_3 and TiO_2 supports allowed the imaging of the active catalyst and enabled a precise determination of the Au particle size distribution and particle shape using transmission electron microscopy (TEM). Further, the apparent

reaction orders and the stretching frequency of CO adsorbed on Au^0 (near 2100 cm^{-1}) determined by diffuse reflectance infrared spectroscopy (DRIFTS) depend on d. Because of the changes in reaction rates, kinetics, and the CO stretching frequency with number average Au particle size, it is determined that the dominant active sites are the low coordinated corner Au sites, which are 3 and 7 times more active than the perimeter Au sites for Au/Al_2O_3 and Au/TiO_2 catalysts, respectively, and 10 times more active for Au on TiO_2 versus Al_2O_3. From operando Fourier transform infrared spectroscopy (FTIR) experiments, it is determined that the active Au sites are metallic in nature. In addition, Au/Al_2O_3 catalysts have a higher apparent H_2O order (0.63) and lower apparent activation energy (9 kJ mol^{-1}) than Au/TiO_2 catalysts with apparent H_2O order of −0.42 to −0.21 and activation energy of 45−60 kJ mol^{-1} at near 120 °C. From these data, we conclude that the support directly participates by activating H_2O molecules.
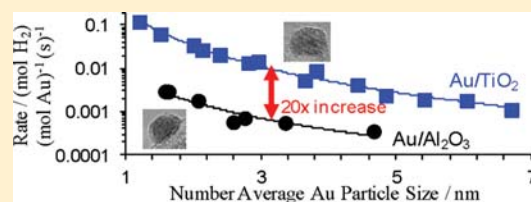
■ INTRODUCTION

Oxide supported Au nanoparticles are known to catalyze various reactions, both in the liquid and in the gas phase, whereas bulk Au is regarded to be inert. Thus, a study of the origin of the catalytic activity of supported Au nanoparticles is ideal to identify the unique features of the metal nanoparticles as compared to those of their bulk. The source of the catalytic activity of supported Au nanoparticles has been claimed to be cationic Au,[1] bilayers of Au,[2,3] perimeter sites,[4] and low coordinated corner sites.[5,6] While the nature of active sites of supported Au nanoparticles is still being debated, most studies indicate that only a small fraction of the total Au provides most of their catalytic activity.[1−6]

The effect of support on catalytic performance is said to originate from either a direct participation of the support[7,8] or an indirect role, by influencing the shape and size of the metal nanoparticles,[6] by charge transfer from or to the metal nanoparticles,[9] by metal support interactions,[10] or by stabilizing ionic metal species.[11] The reducibility[7] and the oxygen storage capacity[12] of the support material have been shown to be the descriptors that govern their catalytic properties. Au nanoparticles supported on TiO_2 have been shown to have higher catalytic rates than those supported on Al_2O_3 in the oxidative

environment of CO oxidation[6,13] and the reducing atmosphere present during the water−gas shift (WGS) reaction.[14] WGS is an important industrial chemical process for the production of hydrogen and plays a role in the production of methanol, each of which may be directly used as a fuel for various applications. The WGS reaction has been previously studied on model Au/TiO_2(110) catalysts.[8] On the basis of experimental and theoretical studies, a reaction mechanism that involves a cooperative interaction between Au and TiO_2 where each catalyzes different steps of the WGS reaction has been proposed.[8]

To gain insights into the unique features of metal nanoparticles and the effect of support material on their catalytic properties, we report here a kinetic and spectroscopic investigation of the WGS reaction over Au nanoparticles of different average sizes supported on Al_2O_3 and TiO_2. Model, nonporous and crystalline, Al_2O_3 and TiO_2 supports are used for the study. Nonporous supports allow the imaging of the active Au because all of the Au is exposed on the surface of the support. Crystalline supports provide enhanced contrast between the metal nanoparticles and the support in transmission electron

microscopy (TEM) images. The Au/Al$_2$O$_3$ and Au/TiO$_2$ catalysts used for the study had a narrow particle size distribution of Au nanoparticles, and to eliminate the errors associated with using an average Au particle size, the entire Au particle size distribution identified by TEM was used to reach the conclusions in our work. While the variation of the WGS reaction kinetics with nanoparticle size is used to determine the active sites of Au/Al$_2$O$_3$ and Au/TiO$_2$ catalysts, the variation of the WGS reaction kinetics with support material is used to determine the cause of the effect of support.

■ EXPERIMENTAL METHODS

Catalyst Preparation. The Au/Al$_2$O$_3$ and Au/TiO$_2$ catalysts were prepared by the deposition precipitation (DP) method. Nonporous Al$_2$O$_3$ and rutile TiO$_2$ supports were used to ensure that all Au is deposited on the outside of the support, and is thus accessible to imaging. The Al$_2$O$_3$ support used was corporation lot number A30U045 from Alfa Aesar and is nonporous with a BET surface area of 33 m^2 per gram. The rutile TiO$_2$ support used was corporation lot number E3-692-011-005 from Sachtleben Chemie GmbH, Germany, and is nonporous with a stable BET surface area of 28 m^2 per gram (after steaming at 500 °C using a 30% water in air mixture for 48 h). The Au precursor (99.99% HAuCl$_4$·3H$_2$O from Alfa Aesar) was added to deionized water to give a 0.0015 M gold solution. A solution of 0.1 N NaOH was added dropwise to the Au solution so that the solution maintained a pH = 6 at 35 °C for approximately 6 h. The support material (Al$_2$O$_3$ or TiO$_2$) was then added to the solution, and the mixture was heated to 85 °C in 30 min. The mixture was maintained at 85 °C for 1 h. The mixture was then cooled, centrifuged, washed, and dried. The procedure is detailed in our previous work.[5] Concentrations of Au were determined by comparing results to those of known standards by atomic absorption spectroscopy, performed on each sample using an AAS, Perkin-Elmer AAnalyst 300 instrument.

TEM. The imaging advantages of having high Z contrast between a metal and its nonporous support are clearly shown in Figure 1. The
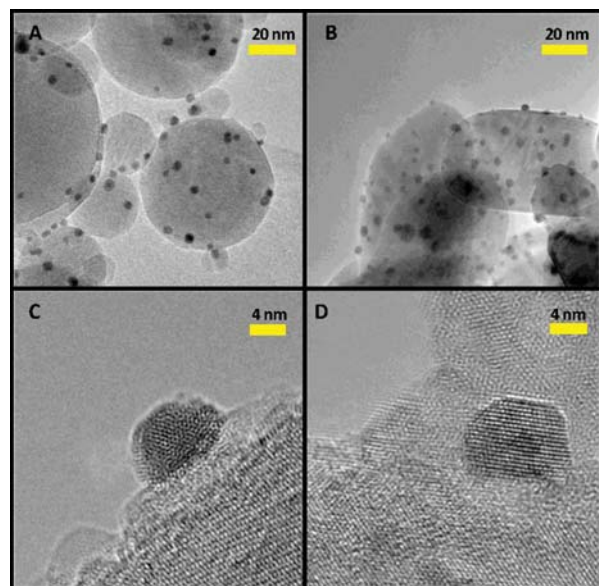
size can change due to sintering. Prior to the experiments, the catalyst samples were dispersed in ethanol and sonicated for 10 min. The suspensions were then dropped on 200 mesh lacey carbon-coated copper grids. The grids were dried in air for 15 min at room temperature. All prepared samples were investigated using an 80−300 kV S/TEM FEI Titan operating at 300 kV. Each gold cluster size was determined from the longest measurable distance for that cluster. From conventional TEM, it was possible for us to observe Au nanoparticles as low as 0.8 nm in size. The number (d), surface (d_s), and volume (d_v) average Au particle sizes were then determined. The calculations of average Au particle sizes are detailed in the Supporting Information. Figure S1 shows that the difference between the values of d, d_s, and d_v for Au/Al$_2$O$_3$ catalysts is small, indicating a narrow Au particle size distribution on these catalysts. Further, to eliminate the errors associated with using an average Au particle size, the contribution of the entire Au particle size distribution identified by TEM, for all of the Au/Al$_2$O$_3$ and Au/TiO$_2$ catalysts used for the study, to the WGS reaction rate was used to reach conclusions in this work. This methodology is explained in detail in the Supporting Information.

Au-Edge Extended X-ray Absorption Fine Structure (EXAFS) Measurements. The X-ray absorption measurements were made on the insertion device beamline of the Materials Research Collaborative Access Team (MRCAT) at the Advanced Photon Source, Argonne National Laboratory. Prior to the EXAFS measurements, the Au catalysts used in the kinetic experiments were rereduced at 200 °C for 30 min in 4% H$_2$/He followed by He purge at 200 °C, and cooled to room temperature in a continuous-flow EXAFS reactor cell. The spectra were obtained at room temperature under static He atmosphere. Catalyst samples were pressed into a cylindrical holder with a thickness chosen to give a total absorbance (μx) at the Au L$_3$ (11.919 keV) edge of about 2.0 and a Au edge step ($\Delta\mu x$) of ca. 0.5. The measurements were made in transmission mode with the ionization chambers optimized for the maximum current with linear response ($\sim$1010 photons detected s^{-1}). A mixture of N$_2$ and He in the incident X-ray detector and a mixture of ca. 20% Ar in N$_2$ in the transmission X-ray detector were used. A third detector in the series collected a Au foil spectrum simultaneously with each measurement for energy calibration. Phase shifts and backscattering amplitudes were obtained from the Au foil for Au−Au.

Operando Fourier Transform Infrared (FTIR) Spectroscopy. The FTIR spectrometer used a Bruker Vertex 70 FTIR, and the transmission IR cell is a homemade reactor. The IR reactor cell consists of a central stainless steel hollow cylinder with 4.76 cm o.d. and 3.00 cm i.d. About 70 mg of catalyst sample for the transmission IR study was pressed in the form of a thin wafer with diameter about 2 cm. The catalyst sample wafer in the IR cell was placed between two indented sample holders with three gas flow channels to guide the reaction gas mixture flow through the wafer. Two CaF$_2$ windows were used for the IR cell and were 2.54 cm in diameter and 1.00 cm in thickness. Two custom-made beveled graphite ferrules (Chromalytic Technology Pty Ltd., Australia) with 3.00 cm o.d., 2.56 cm i.d., overall length 0.6 cm, bevel length 0.42 cm were used to seal the gap between the CaF$_2$ window and IR cell body. A K-type thermocouple was placed within the IR cell so that its tip touched the edge of the sample holders. The IR backgrounds of 100 scans were collected when the catalyst was exposed to the 11% H$_2$O balanced in Ar and He. All spectra were collected at a resolution of 4 cm^{-1} and averaged over 50 scans. For the operando studies, the CO, H$_2$, Ar balanced in He were bubbled through a H$_2$O saturator heated to a temperature at which the vapor pressure gave the desired concentration. The concentrations of these gases, except for H$_2$O and CO$_2$, were the same as for the kinetic measurements done in the tubular reactor unit in this study. The total flow rate was 50 sccm, and all lines were heat traced with heating tape and covered with insulation and aluminum foil to prevent condensation of the water vapor. The gas stream coming out from the IR reactor cell was periodically injected into an Agilent 5890 gas chromatograph (GC) equipped with a thermal conductivity detector (TCD) and a Carboxen 1000 column.

The catalyst loaded into the IR reactor cell was the fresh catalyst from the same batch used in kinetic study. It was pretreated with the

Figure 1. (A,B) Typical TEM images of Au/Al$_2$O$_3$ and Au/TiO$_2$ catalysts, respectively, used to determine the Au particle size distributions. (C,D) Typical HR-TEM images of Au/Al$_2$O$_3$ and Au/TiO$_2$ catalysts, respectively, used to determine the particle shape.

use of the nonporous support also ensures that no metal clusters are hidden from view within a pore structure. TEM images were obtained for the used catalysts after the WGS experiments because Au particle

same procedure as used in the kinetic study. Throughout all of the experiments, the total flow rate of gases through the IR cell was kept constant at 50 sccm. The IR spectra and concentration measurements by GC during the stabilization and under steady-state reaction conditions were collected when the sample was at 200 °C. Integration of the IR peak areas under the linearly bound CO on Au peaks was completed with CasaXPS version 2.3.12. Gaussian−Lorentzian symmetric line-shape curves, GL (30), that is, 70% Lorentzian and 30% Gaussian, were used, and the peak position, area, and full width at half maximum (fwhm) are optimized by minimizing the root-mean-square (rms) error through Levenberg−Marquardt iterations (in CasaXPS).

Kinetic Measurements − Tubular Reactor Unit. For each of the kinetic experiments, 100−1300 mg of catalyst was added to the reactor. A description of the automated, four independent parallel tubular plug flow reactor setup is available elsewhere.[15] The catalysts were reduced in a 25% H_2, 75% Ar mixture with a flow rate of 50 sccm followed by a pretreatment at the standard WGS conditions (6.8% CO, 21.9% H_2O, 8.5% CO_2, 37.4% H_2, and balance Ar) with a flow rate of 75.4 sccm at the temperatures shown in Tables S1−S4. After this WGS pretreatment, the temperature was lowered so that conversion was less than 10%, and the initial WGS rates were determined. The results in Tables S1−S4 show that exposing the catalysts to reduction followed by WGS conditions at increasingly elevated temperatures resulted in increased average gold particle size. In addition, by keeping the weight loading of gold low and minimizing exposure of the catalysts to WGS conditions, it was possible to maintain small particle sizes. Thus, it was possible to examine the effect of the Au particle size distribution on the rate. For uniformity, the initial rate after pretreatment was used in the results shown in Table S1, Figure 2, and Figure 3 for the comparison of all of the samples.
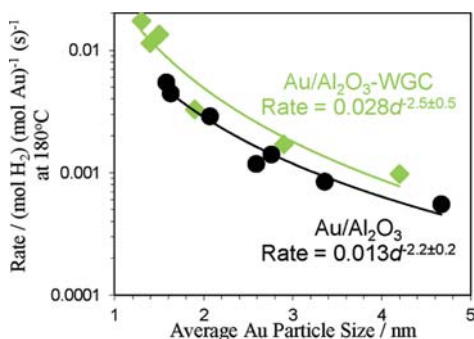

Figure 2. Rate per total mole of Au calculated at 180 °C, 6.8% CO, 21.9% H_2O, 8.5% CO_2, and 37.4% H_2 for Au/Al_2O_3-WGC (◆) and Au/Al_2O_3 (●) catalysts versus average Au particle size determined by EXAFS and number average Au particle size determined by TEM, respectively. The vertical dimensions of the points represent the 15% error associated with rate measurement.

To determine the apparent activation energy, the temperature was varied over a range of 30 °C, with the concentrations kept at standard conditions. The apparent reaction orders with respect to the reactants and products were measured by varying one gas concentration at a time. The four concentrations were varied over the ranges 4−21% CO, 5−25% CO_2, 11−34% H_2O, and 14−55% H_2. After the kinetic experiments, the catalysts were exposed to Ar gas as the temperature was lowered to room temperature. Once at room temperature, the catalysts were passivated with a 2% O_2 in Ar mixture for 2 h. A more detailed discussion of the procedure for the WGS kinetic measurements is provided in our earlier work.[5]

■ RESULTS

Determination of Au Particle Size by TEM. The Au particle size distribution and particle shape of Au nanoparticles supported on Al_2O_3 and TiO_2 were determined using TEM images of used catalysts. Figure 1A and B shows typical images
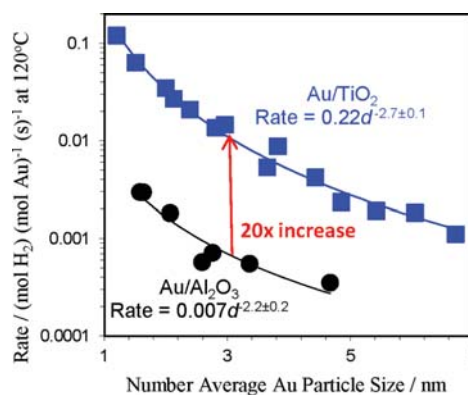

Figure 3. Rate per total mole of Au calculated at 120 °C, 6.8% CO, 21.9% H_2O, 8.5% CO_2, and 37.4% H_2 for Au/Al_2O_3 (●) and Au/TiO_2 catalysts (■) versus number average Au particle size. The vertical dimensions of the points represent the 15% error associated with rate measurement.

that were used to measure the Au particle size distribution for Au/Al_2O_3 and Au/TiO_2 catalysts, respectively. While Figure 1A and B shows the representative TEM images of the catalysts that possess Au nanoparticles with average particle size greater than 4 nm, Figure S2 gives representative TEM images of the catalysts that possess Au nanoparticles with average particle size less than 2 nm. Measurements of number average Au particle size and its standard deviation for Au/Al_2O_3 catalysts are reported in Table S1. Examples of the high resolution (HR)-TEM images that were used to determine the shape of the Au nanoparticles with a particle size greater than 2 nm supported on Al_2O_3 and TiO_2 are shown in Figure 1C and D, respectively. The geometry of Au nanoparticles with a particle size less than 2 nm supported on TiO_2 is shown in the representative high-angle annular dark-field (HAADF) scanning transmission electron microscopy (STEM) images in our earlier work.[5] Because it was only possible for us to observe Au nanoparticles as low as 0.8 nm in size by conventional TEM, HAADF STEM images were also used[5] to calculate the density of subnanometer Au particles on Au/TiO_2 catalysts. However, these subnanometer Au particles were not found in sufficient numbers to account for significant catalytic activity.[5] This finding can be extended to Au/Al_2O_3 catalysts because, as will be discussed later, they exhibit similar dependence of the WGS reaction rate with average Au particle size to Au/TiO_2 catalysts. Therefore, the density of subnanometer Au particles on Au/Al_2O_3 catalysts was not determined. The World Gold Council (Au/Al_2O_3-WGC) catalysts were not imaged by TEM. The average particle size range of the Au/Al_2O_3 and Au/TiO_2 catalysts studied in this work is 1−5 and 1−7 nm, respectively. This particle size range is similar to the size range studied by other researchers.[1,2,4−6,8,17]

Determination of Au Particle Size by Au-Edge EXAFS Measurements. The average Au particle size of Au/Al_2O_3-WGC catalysts was determined by EXAFS because they were not amenable to high-resolution measurements by TEM. WINXAS97 software was used to analyze the EXAFS data. The coordination parameters were obtained by a least-squares fit in r-space of the k^2-weighted Fourier transform data. The EXAFS particle size was determined from the previous correlation of coordination number with particle size.[16] Because the coordination number is correlated to $\Delta\sigma^2$, or the Debye−Waller factor (DWF), calibration of the DWF was obtained by determination of the average particle size from TEM for several

Au/Al_2O_3 catalysts. The EXAFS data for these catalysts were fit using the coordination number appropriate for that particle size. Once the best fit DWF was determined for these catalysts, this value was used in the fits of the other catalysts. The DWFs (and coordination numbers) determined from the fixed coordination number fits were not significantly different from values determined from standard fits with unconstrained coordination numbers. Table S1 summarizes the average Au particle sizes on Au/Al_2O_3 catalysts obtained by EXAFS. The EXAFS fits are shown in Table S2. Because of the calibration of the DWF, there is a good agreement between the number average Au particle sizes measured by TEM and those calculated from the EXAFS fitting for the Au/Al_2O_3 catalysts. For Au/Al_2O_3 catalysts, the Au–Au bond distance by EXAFS varies from 2.75 Å at lower average Au particle sizes to 2.84 Å at higher average Au particle sizes (Table S2). This decrease in bond distance has been attributed to the increase in d-electron density of Au atoms in small particles.[16] In our model, we assume that the TOR of the low coordination corner and perimeter sites are not significantly affected by this change.

Kinetic Studies on Au/TiO_2 and Au/Al_2O_3 Catalysts. The WGS reaction rate per total mole of Au over Au/Al_2O_3 catalysts is reported in Table S1. The corresponding data for Au/TiO_2 catalysts were reported in our previous work.[5] The WGS reaction rate per total mole of Au of Au/Al_2O_3 catalysts at 180 °C varies from 5.5×10^{-3} mol H_2 (mol Au)$^{-1}$ s^{-1} at a number average Au particle size of 1.6 nm to 0.6×10^{-3} mol H_2 (mol Au)$^{-1}$ s^{-1} at a number average Au particle size of 4.7 nm. The WGS reaction rate per total mole of Au of Au/Al_2O_3-WGC catalysts at 180 °C varies from 17.3×10^{-3} mol H_2 (mol Au)$^{-1}$ s^{-1} at an average Au particle size of 1.3 nm to 1.0×10^{-3} mol H_2 (mol Au)$^{-1}$ s^{-1} at an average Au particle size of 4.2 nm. Figure 2 shows that the WGS reaction rate per total mol of Au varies as $d^{-2.2\pm0.2}$ for Au/Al_2O_3 catalysts. This is in agreement with the dependence of $d^{-2.5\pm0.5}$ obtained for Au/Al_2O_3-WGC catalysts. The data for Au/Al_2O_3-WGC catalysts are relatively scattered due to a lower precision of EXAFS for measurement of the average Au particle size. On average, the Au/Al_2O_3-WGC catalysts have 2 times higher WGS reaction rate per total mol of Au as compared to Au/Al_2O_3 catalysts at 180 °C and the same average Au particle size. In a previous paper from our group,[5] a particle size dependence of $d^{-2.7\pm0.1}$ was reported for a series of Au/TiO_2 catalysts. Similar particle size dependence of the reaction rate per total mole of Au has been reported in the literature[6,17] for CO oxidation on Au catalysts. Figure 3 shows a comparison of catalytic activity of Au/TiO_2 and Au/Al_2O_3 catalysts over a number average Au particle size range of 1−7 nm calculated at 120 °C. The rate and apparent activation energies of Au/Al_2O_3 catalysts were measured at 170−200 °C. For comparison with Au/TiO_2 catalysts, this rate was extrapolated to 120 °C by assuming that the apparent activation energy does not vary in the temperature range 120−200 °C. Figure 3 enables us to compare the WGS reaction rate per total mol of Au for Au/Al_2O_3 and Au/TiO_2 catalysts at the same number average Au particle size and clearly shows that Au/TiO_2 catalysts have ∼20 times higher WGS reaction rate per total mole of Au than Au/Al_2O_3 catalysts at 120 °C when compared at the same number average Au particle size.

Figure S3 shows typical plots used in the determination of apparent reaction orders for CO, CO_2, H_2, and H_2O for Au/Al_2O_3 and Au/TiO_2 catalysts. Au catalysts, irrespective of the support, show an apparent CO order ∼1, apparent CO_2 order ∼0, and a slightly negative apparent H_2 order. The apparent H_2O order varies considerably with a change in support when compared at the same temperature. The apparent H_2O order is 0.63 for Au/Al_2O_3 catalysts at 130 °C and ranges from −0.42 to −0.21 for Au/TiO_2 catalysts at 120 °C. The apparent reaction orders also show a subtle variation with number average Au particle size, the implications of which are discussed below. Figure S4 shows the trend that Au/Al_2O_3 catalysts typically have lower apparent activation energies (5−20 kJ mol^{-1}) than those of Au/TiO_2 catalysts (40−60 kJ mol^{-1}). The values of apparent kinetic parameters measured on Au/Al_2O_3 and Au/TiO_2 catalysts are reported in Tables S3 and S4, respectively.

Operando FTIR Spectroscopy. The operando FTIR spectra recorded during deactivation of Au/Al_2O_3 catalysts with time and their analyses are shown in Figure S5 and Figure 4,
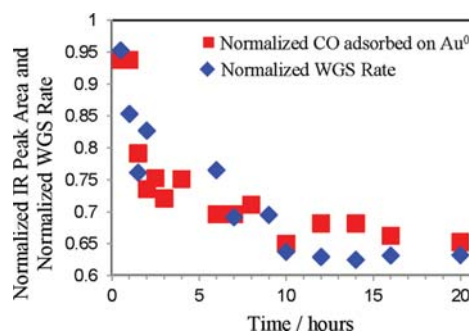

Figure 4. Analysis of operando FTIR data of WGS reaction; normalized WGS rate (◆) and normalized CO adsorbed on Au^0 (■) versus time for Au/Al_2O_3 catalysts.

respectively. The peak at 2100 cm^{-1} was assigned to CO adsorbed on metallic Au. The normalized area of this peak varies linearly with the normalized WGS rate. These results are similar to those reported in our previous diffuse reflectance infrared spectroscopy (DRIFTS) study on Au/TiO_2 catalysts[5] and the literature on Au/$CeZrO_4$ catalysts.[18] Unlike for the Au/TiO_2 catalysts,[5] no IR peak at 2050 cm^{-1} was observed on the Au/Al_2O_3 catalysts. Also, on the alumina-supported catalysts, no peak was observed for CO adsorbed on positively charged Au. The IR peaks corresponding to formate and carbonate species show either an inverse or no correlation with the WGS reaction rate on Au/Al_2O_3 (Figures S5A, S5B, and S5C) and Au/TiO_2 catalysts. Figure S5D shows that the fluctuations in the water background were large as compared to the smaller intensities of OH groups adsorbed on the surface. Therefore, the OH content of the Al_2O_3 and TiO_2 used in the experiments could not be quantified.

■ DISCUSSION

Active Sites. The WGS reaction rates are often normalized by the total amount of surface metal to obtain a turnover rate (TOR).[19,20] It has been shown[21] that such a WGS TOR is independent of weight loading and metal particle size for Pt/Al_2O_3, Pt/TiO_2, and Pt/CeO_2 catalysts. Thus, it can be concluded that each surface Pt atom has the same WGS reaction rate for these catalysts. For Au catalysts, however, we do not know of a way to determine the total amount of surface Au sites by chemisorption. Hence, we report a WGS reaction rate normalized by the total moles of Au in the catalyst. For particles with regular geometries, the total amount of surface Au sites varies approximately with number average Au particle size (d) as d^{-1}. Thus, the rate per total mole of Au should vary as d^{-1} for

the TOR to be independent of Au particle size if all of the surface Au sites are uniformly active. In our previous work,[5] we have shown that the WGS reaction rate per total mole of Au varies as $d^{-2.7\pm0.1}$ for Au/TiO$_2$ catalysts at 120 °C. For Au/Al$_2$O$_3$ catalysts, however, the WGS reaction rate per total mole of Au varies as $d^{-2.2\pm0.2}$ at 180 °C. Hence, the TOR, normalized to surface Au, for Au/TiO$_2$ and Au/Al$_2$O$_3$ catalysts varies approximately as $d^{-1.7}$ and $d^{-1.2}$, respectively. The changes in TOR with Au particle size show that each surface site does not exhibit the same rate. Au nanoparticles have been shown experimentally and theoretically[6] to have energetically heterogeneous Au sites. The CO and O surface species bind more strongly on Au sites with lower Au–Au coordination number. Previously, a physical model of Au clusters as truncated cuboctahedra (Figure 5) was developed.[5] This model was used to determine how the number of different types of sites, which have different Au–Au coordination number, varies with Au particle size (Figure 5). The model, in conjunction with the
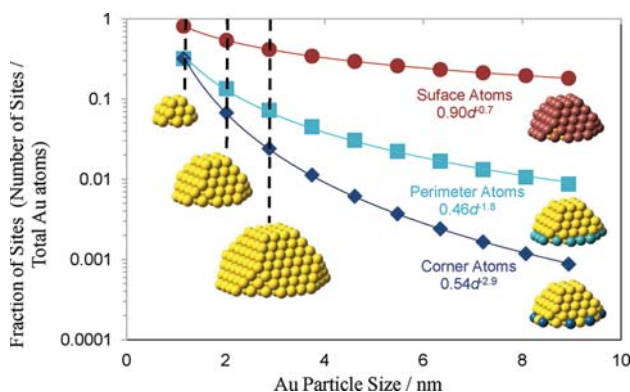

Figure 5. Variation of the fraction of surface sites (red), perimeter sites (green), and low coordinated corner sites (blue) with Au particle size in truncated cuboctahedra geometry. Similar models are detailed in the literature.[22]

variation of WGS reaction rate per total mole of Au with Au particle size distribution for Au/TiO$_2$ catalysts, was used to determine the dominant active site. It was assumed that the rate per active site is independent of Au particle size. A rate for each sample was calculated from the following equation:

$$ r = \left[\sum c_{\text{site}} s(d) \right] / \left[\sum t(d) \right] $$

where $s(d)$ is the WGS reaction rate per total mole of Au, $s(d)$ is the number of atoms for a cluster of diameter d that corresponds to the site of interest, $t(d)$ is the total number of atoms for that cluster, and the summation was carried out over all of the Au particles identified from the TEM image of that catalyst. In other words, the full Au particle size distribution was used for each sample. The constant, c_{site}, was calculated from a best fit of the model to the experimental rate data over the full range of number average Au particle sizes represented by all 14 samples studied. For Au nanoparticles supported on model TiO$_2$, the corner site was found to be the dominant active site. A similar result for CO oxidation reaction has been reported in the literature on Au catalysts.[6,17] It was noted that allowing for multiple sites to contribute to the rate improved the fit to the data.[5] Further, the model could not distinguish between the corner sites that have contact with the support having an Au–Au coordination number of 4 from

those without support contact having an Au–Au coordination number of 6.

The HR-TEM images indicate that the Au nanoparticles supported on model Al$_2$O$_3$ also have truncated cuboctahedra geometry (Figure 1). This allows us to use the same physical model of Au nanoparticles as truncated cuboctahedra for the determination of active sites for these catalysts. The rate per total mole of Au for Au/Al$_2$O$_3$ catalysts varies as $d^{-2.2\pm0.2}$, whereas the surface sites vary as $d^{-0.7}$, the perimeter sites vary as $d^{-1.8}$, and the corner sites vary as $d^{-2.9}$ (Figure 5). Thus, if only one site is considered to be active, that is, the model used in our previous work,[5] the variation in the WGS reaction rate per total mole of Au does not correlate well with either the surface or the perimeter or the corner sites as the dominant active site. Therefore, a model that assumes multiple sites to be active was created to better understand the particle size dependence. The WGS reaction rate per total mole of Au for each catalyst is considered to be a sum of rates of the corner sites (in contact with the support), the rest of the perimeter sites (in contact with the support), and the rest of the surface sites (not in contact with the support), according to the equation:

$$ r = \sum \left[x_c(d)R_c + x_p(d)R_p + x_s(d)R_s \right] $$

These sites are defined such that they are mutually exclusive; that is, the perimeter sites do not include the corner sites, and the surface sites do not include either the perimeter or the corner sites. Here, r is the WGS reaction rate per total mole of Au, $x_c(d)$, $x_p(d)$, and $x_s(d)$ are the fractions of corner, perimeter, and surface sites calculated from truncated cuboctahedra geometry, respectively. R_c, R_p, and R_s are the turnover rates (mole H$_2$ produced per mole corner, perimeter, and surface site, respectively). R_c, R_p, and R_s are assumed to be independent of Au particle size. This assumption is based on density functional calculations from which it is suggested that the most important factor affecting the adsorption and reaction properties of Au sites is their coordination with the other atoms.[23] The summation was carried out over all of the Au particles identified from the TEM image of that catalyst. The inclusion of the entire particle size distribution of all of the Au/Al$_2$O$_3$ catalysts tested at 180 °C in this model eliminated the errors associated with using an average Au particle size as explained in more detail in the Supporting Information. The model involved three parameters, R_c, R_p, and R_s, which were linearly optimized with seven data points on Au/Al$_2$O$_3$ catalysts tested at 180 °C. The results of the model indicate that at 180 °C, $R_c = 3R_p \gg R_s \approx 0$. R_c is computed to be 0.04 mol product H$_2$ (mole corner Au)$^{-1}$ (s)$^{-1}$ at this temperature. The optimal value of R_s is 3 orders of magnitude lower than R_c and R_p. A similar analysis (i.e., the model developed here considering multiple sites to be active) was done on Au/TiO$_2$ catalysts. The model involved three parameters, R_c, R_p, and R_s, which were linearly optimized with nine data points, on Au/TiO$_2$ catalysts tested at 120 °C, reported elsewhere.[5] The model gives the result that at 120 °C, $R_c = 7R_p \gg R_s \approx 0$, with R_c computed to be 0.5 mol product H$_2$ (mole corner Au)$^{-1}$ (s)$^{-1}$ at this temperature. Again, the optimal value of R_s is 3 orders of magnitude lower than R_c and R_p. A parity plot, indicating the goodness of these fits, is shown in Figure S6. A porous pure Au catalyst, with a BET surface area of 0.8 m^2 g^{-1}, the details of preparation of which can be found elsewhere,[24,25] was tested to investigate the WGS activity of bulk Au. Its WGS reaction rate per total mole of Au was found to be 5.7 × 10^{-6} mol H$_2$

(mol Au)$^{-1}$ s^{-1} at 200 °C. This result reinforces the idea that the surface Au sites are inactive ($R_s \approx 0$). This residual activity may be coming from Ag leftover from the preparation.

It has been argued that Au sites in contact with the support (corner sites and perimeter sites having a Au−Au coordination number of 4 and 5, respectively) will be inactive due to the increased coordination provided by the support.[26] Also, it is noted that the inclusion of corner sites without support contact having a Au−Au coordination number of 6 and/or the defect sites in the model can give an equally good fit to the experimental data of Au/Al$_2$O$_3$ and Au/TiO$_2$ catalysts. However, these sites are away from the support, making them unlikely to account for the order of magnitude difference in rates and kinetic parameters and the changes in reaction order for Au/TiO$_2$ versus Au/Al$_2$O$_3$ catalysts. Therefore, in the model, all of the sites without support contact are lumped into the surface sites. Further, it should be noted that an inherent assumption in calculating the TORs of corner sites (R_c), perimeter sites (R_p), and surface sites (R_s) is that reaction step(s) occurring on the Au nanoparticles is(are) kinetically relevant. The sharp dependence ($d^{-2.2}$ and $d^{-2.7}$ for Au/Al$_2$O$_3$ and Au/TiO$_2$, respectively) of the WGS reaction rate on number average Au particle size implies that the rate is limited by the total amount of Au sites. We note that there could also be kinetically significant steps that occur on the oxide support, but the number of these sites does not change as the Au particle size is varied. That such sites on the support can contribute to the rate is shown by density functional computations in the work by Sanz et al.[8]

Figure 6 shows that the apparent reaction orders vary with number average Au particle size on Au/Al$_2$O$_3$ and Au/TiO$_2$ catalysts. These variations are smaller as compared to the

variations that are due to the change of support, but are further evidence that there exist multiple active sites contributing significantly to the rate. This is because the energetically different corner and perimeter sites are likely to have different inherent apparent reaction orders. However, the apparent reaction orders that we measure are a combination of the two. From the results of the model, the rate per corner site is 3 and 7 times larger than the rate per perimeter site for Au/Al$_2$O$_3$ and Au/TiO$_2$ catalysts, respectively. However, in large Au nanoparticles, the number of perimeter sites is much greater than the number of corner sites. Thus, the perimeter sites, despite their lower rates, can contribute significantly to the overall rate. The percentage contribution of perimeter sites to the overall rate at a particular Au particle size can be calculated by using the equation:

$$\text{rate by perimeter } (d) = \frac{\sum x_p(d) R_p}{\sum x_p(d) R_p + \sum x_c(d) R_c} \times 100\%$$

Here, $x_c(d)$ and $x_p(d)$ are the fraction of corner and perimeter sites, respectively, calculated from truncated cuboctahedra geometry. R_c and R_p are rates per mole corner and perimeter sites, respectively. R_s, the rate on the surface sites, is taken to be zero as discussed above. The summation was carried out over all of the Au particles identified from the TEM images of that catalyst. The results indicate that for the Au/Al$_2$O$_3$ catalysts, the perimeter sites contribute 13% of the total rate at 1.6 nm number average Au particle size and 55% at 4.7 nm number average Au particle size (Table S1). Similar analysis on Au/TiO$_2$ catalysts shows that the perimeter sites contribute 13% at 2.1 nm number average Au particle size and 44% at 6.1 nm number average Au particle size (Table S4). For all of the catalysts tested for apparent reaction orders, the perimeter sites contribute significantly to the overall rate. Thus, a variation in apparent reaction orders with number average Au particle size is expected if the kinetics is distinct in corner versus perimeter sites.

The data shown in Figure 6 can also yield the apparent reaction orders associated with the corner and perimeter sites. By visual inspection, the apparent CO and CO$_2$ orders for Au/Al$_2$O$_3$ catalysts and the apparent CO$_2$ and H$_2$ orders for Au/TiO$_2$ catalysts do not vary with number average Au particle size. The apparent H$_2$ order for Au/Al$_2$O$_3$ catalysts and the apparent CO order for Au/TiO$_2$ catalysts increase with an increase in number average Au particle size, while the apparent H$_2$O order for Au/Al$_2$O$_3$ and Au/TiO$_2$ catalysts decreases with an increase in number average Au particle size. For Au/Al$_2$O$_3$ and Au/TiO$_2$ catalysts with a number average Au particle size of 2.1 nm, the contribution of corner sites to the total rate is 77% and 86%, respectively. Because the majority of the contribution on these catalysts is due to corner sites, the kinetic parameters of these catalysts can be used as an estimate for kinetics parameters of corner sites. Thus, for Au/TiO$_2$ catalysts, the apparent CO order for corner sites is ∼0.63 as compared to >0.84 for perimeter sites. These are in agreement with the idea that the more coordinatively unsaturated corner sites bind CO more strongly and have lower CO order and higher activity. For Au/Al$_2$O$_3$ catalysts, the apparent CO orders associated with corner and perimeter sites are similar (∼0.90). This is in agreement with the corner sites being only 3 times more active than perimeter sites for Au/Al$_2$O$_3$ catalysts. An iterative model with additional parameters was created to determine the
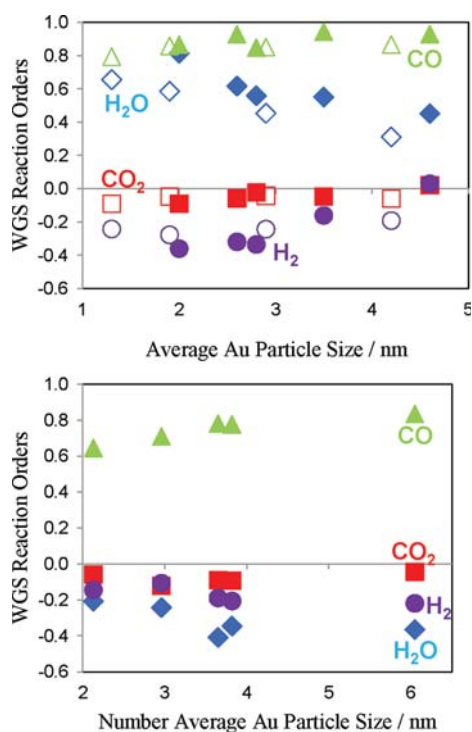

Figure 6. Apparent orders of H$_2$O ($\diamond$, $\blacklozenge$), CO ($\triangle$, $\blacktriangle$), CO$_2$ ($\square$, $\blacksquare$), and H$_2$ ($\bigcirc$, $\bullet$) versus average Au particle size for Au/Al$_2$O$_3$-WGC (open markers) and Au/Al$_2$O$_3$ (filled markers) catalysts at 180 °C (A) and Au/TiO$_2$ catalysts at 120 °C (B).

apparent reaction orders associated with the corner and perimeter sites. The WGS reaction rate data at different partial pressures in the inlet feed were used in conjunction with the already predicted values of R_c and R_p to iteratively optimize for the apparent reaction orders of the corner and perimeter sites for Au/Al$_2$O$_3$ and Au/TiO$_2$ catalysts. Table S5 summarizes the results obtained from the model. On the other hand, the apparent activation energies for Au/Al$_2$O$_3$ and Au/TiO$_2$ catalysts do not vary systematically with the average Au particle size (Tables S3,S4), indicating that the corner and perimeter sites have similar apparent activation energies.

The presence of two energetically distinct CO adsorption sites on Au/TiO$_2$ catalysts is also observed in our in situ DRIFTS spectra.[5] The stretching frequency of the peak near 2100 cm^{-1} (assigned to CO adsorbed on Au^0) for Au/TiO$_2$ catalysts with number average Au particle sizes 2.1, 3.8, and 6.7 nm is 2104, 2109, and 2111 cm^{-1}, respectively. Thus, the stretching frequency of the peak increases with an increase in number average Au particle size. The Blyholder model for the bonding of CO to metals implies that a CO adsorption peak at a higher stretching frequency corresponds to lower back-bonding and CO more weakly bound to the surface.[27] We interpret our DRIFTS data such that the peak near 2100 cm^{-1} is composed of CO adsorbed on corner and perimeter sites. As the number average Au particle size increases, the contribution of perimeter sites to the total rate and thus the amount of CO bound to perimeter sites increases. Because CO binds more weakly to perimeter sites as compared to corner sites, the CO stretching frequency increases with an increase in number average Au particle size. The presence of two energetically distinct CO adsorption sites has also been reported[28] using TPD experiments on Au nanoparticles supported on model flat Al$_2$O$_3$, FeO, and Fe$_3$O$_4$ surfaces. In that work,[28] it was also reported that smaller supported Au nanoparticles bind more strongly to CO, which is in agreement with our findings. Further, IR spectroscopy was used to show[29] that, for Au/TiO$_2$ catalysts, the CO adsorption process on Au^0 (peak near 2100 cm^{-1}) is more complex than that of a single site Langmuir adsorption model. The adsorption data could be better expressed by a two-site Langmuir adsorption model.[29]

The nature of active sites on Au/Al$_2$O$_3$ catalysts was further discerned from operando FTIR experiments. Figure 4 shows that the normalized area of the IR peak at 2100 cm^{-1}, assigned to CO adsorbed on Au^0, varies linearly with the normalized WGS rate. IR peaks corresponding to CO adsorbed on Au$^{\delta+}$ and Au$^{\delta-}$ are not observed on Au/Al$_2$O$_3$ catalysts. In our previous work on Au/TiO$_2$ catalysts,[5] we found that the rate per gram of catalyst was proportional to the 2100 cm^{-1} peak area of CO adsorbed on Au^0, but the 2050 cm^{-1} peak area as well as CO adsorbed on Au$^{\delta+}$ did not correlate with the rate. Thus, the active sites for Au/Al$_2$O$_3$ and Au/TiO$_2$ catalysts are metallic in nature.

In summary, the variation of the WGS reaction rate per total mole of Au with the entire Au particle size distribution determined from TEM was used to determine that the corner and perimeter Au sites in contact with the support are the active sites of Au/Al$_2$O$_3$ and Au/TiO$_2$ catalysts. The presence of multiple active sites was confirmed by the particle-size-driven variation of apparent reaction orders for Au/Al$_2$O$_3$ and Au/TiO$_2$ catalysts and the stretching frequencies of the peak corresponding to CO adsorbed on Au^0 (near 2100 cm^{-1}) in the in situ DRIFTS experiments. These active sites were found to be metallic in nature from operando FTIR data. Thus, we

conclude that the active sites for Au/Al$_2$O$_3$ and Au/TiO$_2$ catalysts are the metallic corner and perimeter Au atoms in contact with the support.

Effect of Support. Numerous studies propose that the reason for the increase in WGS activity on CeO$_2$-supported noble metal catalysts in comparison to Al$_2$O$_3$ supported catalysts is due to the direct participation of the support through either a redox[30,31] or a formate[32,33] mechanism. An indirect role of support has also been reported in the literature.[6,34] For Au catalysts, it has been suggested[6] that the support determines the size and shape of the Au nanoparticles, and consequently the amount of low-coordinated Au sites. Au/support interface energy is an important parameter that determines the final shape and size of the Au particles. The interaction between the Au nanoparticles and the Al$_2$O$_3$ support is significantly stronger as compared to that for the TiO$_2$ support,[6] and the authors suggested that the observed lower TOR per corner site for CO oxidation on Au/Al$_2$O$_3$ catalysts is related to a change in particle shape.[6] Figure 1, however, indicates that the shape of Au nanoparticle does not vary significantly with the support. Thus, the difference in particle shape alone cannot explain a 20 times higher WGS reaction rate per total mole of Au nanoparticles supported on TiO$_2$ as compared to Al$_2$O$_3$ at the same number average Au particle size. Further, the kinetic parameters vary substantially with a change in support, implying that it is not only the difference in number of active Au sites that causes the effect of support. It is interesting, however, that the stronger Au−Al$_2$O$_3$ interaction at the interface could contribute to the order of magnitude lower TOR per corner atom found here for Au/Al$_2$O$_3$ versus Au/TiO$_2$ catalysts.

Several studies[9,10] have suggested that the effect of support is a consequence of an electronic effect of the support on Au nanoparticles. In contrast, our IR data show that for both Au/Al$_2$O$_3$ and Au/TiO$_2$ catalysts, the peak corresponding to CO adsorbed on Au^0 has a stretching frequency of ~2100 cm^{-1}. Thus, if there are electronic effects, they are not strong enough to perturb the Au−CO bonding sufficiently to change the CO stretching frequency. It was also concluded[35] that the CO adsorption energy of Au/TiO$_2$ catalysts increases sharply for Au nanoparticles less than 3 nm in size. However, this effect is unlikely to be the major cause of the effect of support because we observe at least an order of magnitude promotion in rate for Au/TiO$_2$ catalysts with number average Au particle sizes above 3 nm as compared to similar sized Au particles on Au/Al$_2$O$_3$ catalysts.

It was concluded elsewhere[14] that the fast conversion of formate species on Au/TiO$_2$ and Au/CeO$_2$, determined by DRIFTS, could be related to the higher activity displayed by these catalysts. However, our operando FTIR data show that the formate species are not involved in the dominant WGS reaction pathway on Au/Al$_2$O$_3$ catalysts.

Our kinetic data suggest that the support plays a direct role in activating H$_2$O. The apparent CO, CO$_2$, and H$_2$ orders do not vary significantly with a change in the support. This indicates that the adsorption of CO, formation of CO$_2$, and formation of H$_2$ occur on Au rather than on the support. The apparent activation energy and H$_2$O order vary most significantly with a change in support. Au/Al$_2$O$_3$ catalysts have a lower apparent activation energy (9 kJ mol^{-1}) than Au/TiO$_2$ catalysts with apparent activation energy of 45−60 kJ mol^{-1} at near 120 °C. Figure 7 shows that the apparent H$_2$O order decreases for supports that exhibit a higher WGS rate at temperatures in the range from 120 to 190 °C. At 130 °C, the apparent H$_2$O order
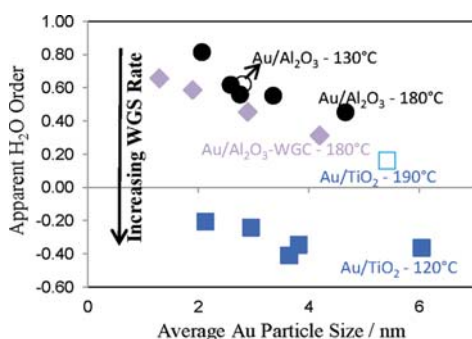
Figure 7. Apparent H_2O order versus average Au particle size for Au/Al$_2$O$_3$-WGC catalysts at 180 °C ($\blacklozenge$), Au/Al$_2$O$_3$ catalysts at 180 °C ($\bullet$) and 130 °C ($\circ$), and Au/TiO$_2$ catalysts at 120 °C ($\blacksquare$) and 190 °C ($\square$).

is 0.63 for Au/Al$_2$O$_3$ catalysts with 2.8 nm number average Au particle size, whereas at 120 °C, the apparent H$_2$O order is −0.36 for Au/TiO$_2$ catalysts with 3.8 nm number average Au particle size. At 180 °C, the apparent H$_2$O order is 0.45 for Au/Al$_2$O$_3$ catalysts with 4.7 nm number average Au particle size, whereas at 190 °C, the apparent H$_2$O order is 0.15 for Au/TiO$_2$ catalysts with 5.4 nm number average Au particle size. The Au/Al$_2$O$_3$-WGC catalysts also follow this trend; they have a slightly lower apparent H$_2$O order and 2 times higher WGS reaction rate per total mole of Au than Au/Al$_2$O$_3$ catalysts at the same average Au particle size. Thus, there is a good correlation between the apparent H$_2$O order and the WGS reaction rate per total mole of Au on different supports at the same average Au particle size and temperature. The variation of H$_2$O order with a change in the support implies the adsorption of H$_2$O occurs on either the support or the Au/support interface.

The apparent reaction orders are related to both the surface concentrations and the adsorption energies. For example, the rate expression for a bimolecular reaction (A + B → products), under the assumption that the reaction proceeds between adjacently adsorbed molecules of A and B, is given by the equation:

$$r = k\theta_A\theta_B$$

where r is the rate, θ_i is the surface coverage by component i, and k is the rate constant. By using the competitive Langmuir adsorption, the rate expression is elaborated to:

$$\theta_i = \frac{K_i P_i}{1 + \sum K_i P_i}$$

where K_i is the adsorption coefficient, P_i is the pressure, and the summation is carried out on A and B, assuming that the products do not adsorb, to give the bimolecular Langmuir–Hinshelwood rate equation:

$$r = \frac{k\, K_A P_A b_B P_B}{(1 + K_A P_A + K_B P_B)^2}$$

The form of this equation predicts that the reactant with higher surface concentration will have a lower apparent reaction order. An apparent order of reaction of about unity implies that this reactant is weakly chemisorbed, and that its surface concentration is near 0; an apparent order of −1 implies that this reactant is strongly held, and its surface concentration is near 1. Therefore, the analysis of the kinetics at a single temperature yields a quantitative picture of the surface concentration and

relative adsorption energies of reactants. A similar discussion is also presented in the literature.[36] Using these arguments, it can be concluded that the lower apparent H$_2$O order on Au/TiO$_2$ catalysts at the same number average Au particle size and temperature as compared to Au/Al$_2$O$_3$ catalysts implies that Au/TiO$_2$ catalysts have a stronger adsorption energy and higher coverage of water/hydroxyl species (O, OH, and H$_2$O). Therefore, the effect of support, that is, an order of magnitude higher TOR of corner sites for Au/TiO$_2$ versus Au/Al$_2$O$_3$, can be attributed to its direct participation in H$_2$O activation. Supports with a higher WGS reaction rate per total mole of Au have higher coverage of hydroxyl species and bind them more strongly. It should be noted that for the catalysts used in our study, the WGS reaction rates are limited by the total amount of Au sites, whereas the total amount of support sites does not change.

■ CONCLUSIONS

The WGS reaction rate per total mole of Au for Au/Al$_2$O$_3$ and Au/TiO$_2$ catalysts varies with the number average Au particle size (d) as $d^{-2.2\pm0.2}$ at 180 °C and $d^{-2.7\pm0.1}$ at 120 °C, respectively. We have used the dependence of the WGS reaction rate per total mole of Au with Au nanoparticle size to determine that the dominant active sites of Au/Al$_2$O$_3$ and Au/TiO$_2$ catalysts are the low coordinated perimeter and corner sites. It is shown that the low coordinated corner Au sites are 3 and 7 times more active than the perimeter Au sites for Au/Al$_2$O$_3$ and Au/TiO$_2$ catalysts, respectively, and that the corner sites are an order of magnitude more active for Au/TiO$_2$ versus Au/Al$_2$O$_3$. From operando FTIR experiments, it has been determined that the active Au sites are metallic in nature. The coordinatively unsaturated perimeter and corner sites are a consequence of the truncated cuboctahedron geometry of the Au nanoparticles. Therefore, to further enhance the catalytic activity of Au catalysts, new nanoparticle shapes that possess sites with Au−Au coordination number less than 4 and a higher fraction of low coordinated sites should be explored.

The WGS reaction rate per total mole of Au for Au/TiO$_2$ catalysts is 20 times higher than that for Au/Al$_2$O$_3$ catalysts at the same number average Au particle size. Because of the variations in apparent H$_2$O order and apparent activation energy with support, it is concluded that the support directly participates in activating H$_2$O molecules. The supports with higher catalytic rates bind water/hydroxyl species more strongly and have a higher coverage of those species. While this conclusion is drawn for the WGS reaction on supported Au nanoparticles, it can be extended to the various catalytic reactions that exhibit the effect of support. Furthermore, this finding poses a challenge to most of the microkinetic modeling efforts for supported metal catalysis because such studies do not take into account the chemistry of the underlying supports in the calculations of activation barriers and adsorption energies. This work implies that including the chemistry of the supports, similar to the work in the literature,[8,37,38] in future microkinetic models may provide more mechanistic insight into the WGS and other reactions catalyzed by supported metal nanoparticles.

■ ASSOCIATED CONTENT

ⓢ Supporting Information

Calculations of number, surface ,and volume average particle size, comparison of our Au/Al$_2$O$_3$ and Au/TiO$_2$ catalysts to the literature, Figures S1−S6, and Tables S1−S6. This material is available free of charge via the Internet at http://pubs.acs.org.

■ AUTHOR INFORMATION

Corresponding Author
fabio@purdue.edu

Present Addresses
[⊥]Center for Functional Nanomaterials, Brookhaven National Laboratory, Upton, New York 11973, United States.
[#]Samsung Electro-Mechanics Co., Ltd., Suwon, South Korea.

Notes
The authors declare no competing financial interest.

■ ACKNOWLEDGMENTS

■ REFERENCES

(1) Fu, Q.; Saltsburg, H.; Flytzani-Stephanopoulos, M. *Science* **2003**, *301*, 935.

(2) Valden, M.; Lai, X.; Goodman, D. W. *Science* **1998**, *281*, 1647.

(3) Herzing, A. A.; Kiely, C. J.; Carley, A. F.; Landon, P.; Hutchings, G. J. *Science* **2008**, *321*, 1331.

(4) Fujitani, T.; Nakamura, I.; Akita, T.; Okumura, M.; Haruta, M. *Angew. Chem., Int. Ed.* **2009**, *48*, 9515.

(5) Williams, W. D.; Shekhar, M.; Lee, W. S.; Kispersky, V.; Delgass, W. N.; Ribeiro, F. H.; Kim, S. M.; Stach, E. A.; Miller, J. T.; Allard, L. F. *J. Am. Chem. Soc.* **2010**, *132*, 14018.

(6) Janssens, T. V. W.; Clausen, B. S.; Hvolbaek, B.; Falsig, H.; Christensen, C. H.; Bligaard, T.; Norskov, J. K. *Top. Catal.* **2007**, *44*, 15.

(7) Schubert, M. M.; Hackenberg, S.; van Veen, A. C.; Muhler, M.; Plzak, V.; Behm, R. J. *J. Catal.* **2001**, *197*, 113.

(8) Rodriguez, J. A.; Evans, J.; Graciani, J.; Park, J. B.; Liu, P.; Hrbek, J.; Sanz, J. F. *J. Phys. Chem. C* **2009**, *113*, 7364.

(9) Sanchez, A.; Abbet, S.; Heiz, U.; Schneider, W. D.; Hakkinen, H.; Barnett, R. N.; Landman, U. *J. Phys. Chem. A* **1999**, *103*, 9573.

(10) Janssens, T. V. W.; Carlsson, A.; Puig-Molina, A.; Clausen, B. S. *J. Catal.* **2006**, *240*, 108.

(11) Costello, C. K.; Kung, M. C.; Oh, H. S.; Wang, Y.; Kung, H. H. *Appl. Catal., A* **2002**, *232*, 159.

(12) Widmann, D.; Liu, Y.; Schuth, F.; Behm, R. J. *J. Catal.* **2010**, *276*, 292.

(13) Arrii, S.; Morfin, F.; Renouprez, A. J.; Rousset, J. L. *J. Am. Chem. Soc.* **2004**, *126*, 1199.

(14) Sandoval, A.; Gomez-Cortes, A.; Zanella, R.; Diaz, G.; Saniger, J. M. *J. Mol. Catal. A: Chem.* **2007**, *278*, 200.

(15) Bollmann, L.; Ratts, J. L.; Joshi, A. M.; Williams, W. D.; Pazmino, J.; Joshi, Y. V.; Miller, J. T.; Kropf, A. J.; Delgass, W. N.; Ribeiro, F. H. *J. Catal.* **2008**, *257*, 43.

(16) Miller, J. T.; Kropf, A. J.; Zha, Y.; Regalbuto, J. R.; Delannoy, L.; Louis, C.; Bus, E.; van Bokhoven, J. A. *J. Catal.* **2006**, *240*, 222.

(17) Overbury, S. H.; Schwartz, V.; Mullim, D. R.; Yan, W. F.; Dai, S. *J. Catal.* **2006**, *241*, 56.

(18) Daly, H.; Goguet, A.; Hardacre, C.; Meunier, F. C.; Pilasombat, R.; Thompsett, D. *J. Catal.* **2010**, *273*, 257.

(19) Koryabkina, N. A.; Phatak, A. A.; Ruettinger, W. F.; Farrauto, R. J.; Ribeiro, F. H. *J. Catal.* **2003**, *217*, 233.

(20) Phatak, A. A.; Koryabkina, N.; Rai, S.; Ratts, J. L.; Ruettinger, W.; Farrauto, R. J.; Blau, G. E.; Delgass, W. N.; Ribeiro, F. H. *Catal. Today* **2007**, *123*, 224.

(21) Panagiotopoulou, P.; Kondarides, D. I. *Catal. Today* **2006**, *112*, 49.

(22) Vanharde, R.; Hartog, F. *Surf. Sci.* **1969**, *15*, 189.

(23) Lopez, N.; Janssens, T. V. W.; Clausen, B. S.; Xu, Y.; Mavrikakis, M.; Bligaard, T.; Norskov, J. K. *J. Catal.* **2004**, *223*, 232.

(24) Ding, Y.; Kim, Y. J.; Erlebacher, J. *Adv. Mater.* **2004**, *16*, 1897.

(25) Erlebacher, J.; Aziz, M. J.; Karma, A.; Dimitrov, N.; Sieradzki, K. *Nature* **2001**, *410*, 450.

(26) Boronat, M.; Illas, F.; Corma, A. *J. Phys. Chem. A* **2009**, *113*, 3750.

(27) Blyholder, G. *J. Phys. Chem.* **1964**, *68*, 2772.

(28) Shaikhutdinov, S. K.; Meyer, R.; Naschitzki, M.; Baumer, M.; Freund, H. J. *Catal. Lett.* **2003**, *86*, 211.

(29) Hartshorn, H.; Pursell, C. J.; Chandler, B. D. *J. Phys. Chem. C* **2009**, *113*, 10718.

(30) Fu, Q.; Deng, W. L.; Saltsburg, H.; Flytzani-Stephanopoulos, M. *Appl. Catal., B* **2005**, *56*, 57.

(31) Rodriguez, J. A. *Catal. Today* **2011**, *160*, 3.

(32) Shido, T.; Iwasawa, Y. *J. Catal.* **1992**, *136*, 493.

(33) Jacobs, G.; Crawford, A. C.; Davis, B. H. *Catal. Lett.* **2005**, *100*, 147.

(34) Zhai, Y. P.; Pierre, D.; Si, R.; Deng, W. L.; Ferrin, P.; Nilekar, A. U.; Peng, G. W.; Herron, J. A.; Bell, D. C.; Saltsburg, H.; Mavrikakis, M.; Flytzani-Stephanopoulos, M. *Science* **2010**, *329*, 1633.

(35) Meier, D. C.; Goodman, D. W. *J. Am. Chem. Soc.* **2004**, *126*, 1892.

(36) Bond, G. C. *Catal. Rev.-Sci. Eng.* **2008**, *50*, 532.

(37) Green, I. X.; Tang, W. J.; Neurock, M.; Yates, J. T. *Science* **2011**, *333*, 736.

(38) Rodriguez, J. A.; Ma, S.; Liu, P.; Hrbek, J.; Evans, J.; Perez, M. *Science* **2007**, *318*, 1757.